

Imaging Radar Observations of Directional Properties of Ocean Waves

WILLIAM MCLEISH AND DUNCAN B. ROSS

*Atlantic Oceanographic and Meteorological Laboratories, National Oceanic and Atmospheric Administration
Miami, Florida 33149*

SEASAT-A synthetic aperture radar (SAR) and side-looking airborne radar (SLAR) images of ocean waves are examined in the form of normalized directional distributions of backscatter variance at series of frequencies. This method provides a more detailed description of radar results than have contoured two-dimensional wave number spectra and reduces some of the uncertainties in relating radar measurements to the waves. The range of aspects of the radar distribution that parallel those of ocean waves is defined. Within this restriction, not only can dominant wave frequencies and directions be determined accurately, but also the shape of a directional peak at a frequency, its directional width, and the background level can be determined approximately. Some of these aspects are examined with SLAR images obtained near reference wave measurements. Through its superior directional resolution, the radar appears to have distinguished two wave trains at a single frequency only 20° different in direction. The SEASAT-A satellite SAR provided an unusual opportunity to examine directional properties of waves in the hostile environment about Hurricane Fico. A swell highly dispersed in frequency and direction at a distance from the center of 450 km had a minimum observed directional width of 11°. Wave directions, their changes with frequency, and directional widths were in accord with those expected from the hurricane winds. Thematic maps of the direction and width of the swell energy as it spread across the ocean surface show smooth changes in these properties over distance, with relatively small scatter of individual values. These patterns also are in accord with those from a simple hurricane wave emission concept, but details of the distributions show distinct departures that must represent unrecognized smaller-scale fluctuations of the process.

INTRODUCTION

High-resolution radar imagery has often shown ocean waves. This observation has led to a number of studies of the relationship between radar images and ocean waves [Alpers *et al.*, 1981]. The patterns are sufficiently similar that Gonzalez *et al.* [1979], Shuchman and Kasischke [1981], and Rosenthal *et al.* [1981] could derive accurate values of the wavelength and direction of dominant ocean waves from satellite radar measurements. However, wave-induced variations in intensity of radar reflectivity may not be simply related to any single property of the waves themselves such as height or slope. McLeish *et al.* [1980] and Beal [1981] observed radar spectra to change with frequency and wave number in a manner between that of wave height spectra and slope spectra. Vesecky and Stewart [1982] found such spectra to agree better with the wave height spectrum, while Pawka *et al.* [1980] reported variable comparisons. Wright *et al.* [1980] found that wave parameters alone did not explain the extent of the radar modulation. Thus, even the nondirectional transfer function relating radar and ocean wave properties is not yet known.

The present effort attempts to derive some properties of hurricane-generated ocean waves from radar measurements without a full knowledge of the transfer relationship. A procedure for presenting the radar spectra as directional distributions that are interpreted within a number of restrictions has been developed. Both side-looking real aperture airborne radar (SLAR) and satellite synthetic aperture radar (SAR) images were analyzed. The SLAR results were tested in part against reference wave measurements. The reference data available to us did not furnish directional distributions of wave energy adequate to evaluate fully those from the SLAR. A more critical test of the radar results has been a comparison of SAR wave

imagery with the unique wind patterns within a hurricane. In this case, the radar-derived directional distributions could be related to the generating wind fields in some detail. In addition, the radar images showed some further directional properties of a swell as it spread across the ocean surface.

In the analysis of SEASAT SAR optically correlated data from a different storm, Gonzalez *et al.* [1982] derived only a dominant wavelength and direction from each spectrum. Although they could show rough relations between the radar-derived wave characteristics and the storm, more detailed interpretation even of the dominant wave field alone produced unsatisfactory results. Considerably finer interpretation is possible from the present digitally correlated data.

PITCH-ROLL BUOY, AIRBORNE SLAR, AND SEASAT SAR WAVE MEASUREMENTS

The general procedures for data collection and analysis follow those given by McLeish *et al.* [1980]. A pitch-roll buoy was used to obtain directional wave measurements from the Canadian ocean station vessel *Vancouver*, which was located at 50°N, 145°W and making routine meteorological observations. Five 34-min wave records obtained on November 17, 1978, between 1811 UT and 2138 UT gave an average spectrum with a frequency interval of 1/128 Hz and 140 degrees of freedom. Unfortunately, there was a slip of the compass card in the buoy, and a direction correction of -50° was applied to the calculated wave directions to produce a fit with the direction of the dominant waves as predicted from weather maps. The correction is estimated to be within 20° of correct.

The analysis procedure calculated a wave height spectrum from the buoy vertical acceleration data. Mean wave directions were obtained using both acceleration and buoy tilt measurements. In addition, two sets of estimates of the directional distribution of wave energy were derived as P in the equation $E(\theta, f) = \cos^{2P(f)} \frac{1}{2}(\theta - \bar{\theta})$ where E is the normalized variance of wave height, θ is direction, and $\bar{\theta}$ is mean direction at the frequency [cf. Longuet-Higgins *et al.*, 1963]. One estimate, P_1 ,

was calculated from the first harmonic of the directional Fourier transform, and the other, P_2 , from the second harmonic. The width of the one-half power peaks was calculated by $W = 4 \cos^{-1} \exp [0.5(\ln 0.5)/P]$.

The SLAR is a Westinghouse APD-7 radar with a 9-mm wavelength and a nominal 8-m resolution cell installed in an aircraft. Two film images produced in conjunction with the buoy measurements of November 17 have been analyzed. One image was obtained at 2047 UT while 14 km E of the ship with an aircraft heading of 142° , and the other was made at 2055 UT while 52 km E-SE of the ship with a heading of 43° . The flight altitude of 52 m led to depression angles varying about 1° . The film segments were digitized, and Fourier analysis was performed on arrays of 128 by 128 values of film density at intervals representing 5.56 m to give two-dimensional wave number spectra with 2 degrees of freedom. Averages of 24 such spectra from each image led to two final spectra with 48 degrees of freedom.

The SEASAT-A satellite operated from July to October 1978 with several microwave instruments that made measurements of the ocean [Born *et al.*, 1979]. The synthetic aperture radar system, useable only when the satellite was in the vicinity of a prepared ground station, quickly demonstrated an ability to image ocean waves [Gonzalez *et al.*, 1979]. Jordan [1980] has described the performance of the instrument. During revolution 251 on July 14, the SAR recorded three successive 100 km by 100 km areas of the ocean surface north of Hurricane Fico. Two-dimensional arrays of readings of backscattered radar energy were produced by a digital correlation technique according to Wu *et al.* [1981]. Digital processing has been reported to give much higher quality radar data than has been produced through optical transform techniques [Vesecky and Stewart, 1982]. The values were spaced at about 17-m intervals and represented a resolution of 25 m. Twelve locations were selected in each image, and 128 by 128 value arrays in 16 areas at each location were used for spectrum calculations. Each resulting average spectrum represented an area of 9 km by 9 km and contained 32 degrees of freedom.

METHODS OF RADAR SPECTRUM ANALYSIS

The radar results in this paper were derived from two-dimensional wave number spectra and are analyzed as normalized directional distributions of radar variance density. Wave numbers were selected to correspond to wave frequencies specified at intervals of 0.01 Hz. This manner of display allows more quantitative examination of radar results than have the contour plots of two-dimensional spectra [cf. Schwab *et al.*, 1981; Gonzalez *et al.*, 1982; Meadows *et al.*, 1983] and either avoids or minimizes several uncertainties in the interpretation of radar data in terms of ocean waves. Through the interpretation methods described herein, a number of properties of ocean waves can be determined from a radar with only a limited knowledge of the applicable transfer function.

A directional distribution of radar variance density was obtained by selecting a series of points along a semicircle on a radar two-dimensional wave number spectrum centered on the origin with a fixed radius representing a selected frequency and with intervals of 1° in direction. Corrections for wave motion, aircraft lateral drift, and radar geometry effects were small and were omitted in these calculations. The variance density at each point was determined by interpolation among the nearest three spectrum values. Each value was divided by the maximum of the series. A resulting value represents the sum of the radar

variance densities from waves propagating in two opposite directions.

Separately normalizing the directional distributions at each frequency removes the effect of frequency dependence of an unknown radar transfer function and simplifies the interpretation of the spectra. Also, with linear waves at a single frequency, the wave height spectrum, the slope spectrum, and some related spectra are all proportional, so that the relative effects of the different wave properties in generating a radar pattern are irrelevant to the directional distributions.

The mean direction of a radar peak at a frequency was determined by averaging by eye the normalized directional distribution in the region between the half-power points. A correction for radar geometry distortion resulting from the difference between horizontal distance and slant range was applied to the mean directions in further calculations from satellite data. The width of a peak is the difference in direction between the one-half power points.

A radar may be expected to show best those waves traveling in the range direction and least well those in the azimuth direction, which is defined as along the flight path [Shuchman and Zelenka, 1978]. The directional transfer function is variable and not well known in a particular case but tends to change smoothly with direction [Alpers *et al.*, 1981, Figure 6] and may not always vary significantly with direction [Elachi, 1978]. The change in this function over a small range of directions must thus be of limited extent. Although the entire 180° range of a radar spectrum semicircle is plotted here, only amplitudes within a single directional peak in a narrow range of directions are compared. In particular, the relative amplitudes of peaks in significantly different directions may not be accurately shown by these directional distributions. The peaks here commonly have widths of 20° – 40° , so that the measurement of a one-half power point requires the use of a range of directions of 10° – 20° . The change in the directional response function over such an interval is considered small. Directional distributions at very low frequencies were not produced, in part because the spectra contain little directional information there and also in order to avoid confusion by patterns not from ocean surface waves, such as wind patterns or internal waves. In addition, a high-frequency limit was selected to be well below that required by resolution cell size to reduce possible aliasing in the calculations.

Although each component of a wave pattern leads to a corresponding component of the radar pattern, the transfer function relating these need not be linear, the superposition of radar components need not parallel that of waves, and the radar form from a sinusoidal wave may not be sinusoidal [Alpers *et al.*, 1981]. However, the Fourier transform of the nonsinusoidal radar pattern reflected from a sinusoidal wave will contain a fundamental component with the same wave number and direction as the wave. Additional radar components will occur as harmonics at multiples of the principal wave number. In order to avoid these harmonics, only frequencies less than $2^{1/2}$ times the frequency of the maximum will be studied in detail here. This restriction avoids the effect of spectrum whitening in frequency described by Alpers *et al.* and ensures that the radar components examined pertain to the intended wave components. Furthermore, the dispersed swell in the third Fico radar image should fit the conditions suggested by Alpers *et al.* for linear radar mapping, and evaluation of the radar results should be possible. Thus, at least with the satellite radar data and under the series of restrictions imposed in the

present calculations, the directional distribution of a radar peak at a frequency should be similar in shape, direction, and width to that of the waves represented.

The presentation of radar spectra as directional distributions is similar to that of *McLeish et al.* [1980]. Directional distributions from radar images were also given by *Pawka et al.* [1980].

SLAR OBSERVATIONS OF WAVES
NEAR BUOY MEASUREMENTS

The 1800 UT surface weather chart (Figure 1) shows a storm south of Alaska as it approached the ship. The reference pitch-roll buoy measurements were collected simultaneously with nearby SLAR-generated imagery of the ocean waves. Winds at the ship were steady from 130° at about 10 m/s at the time; before a weather front passed earlier that day, the direction was 150°, and the wind speed reached 13 m/s. The rapid speed of movement of the storm, also about 13 m/s, requires that dominant waves in the area of the ship resulted from the local wind history and were not swell propagating out from the higher wind regions of the storm.

The buoy-derived wave height spectrum, direction of wave propagation from the first directional harmonics, and the exponents of the cosine distribution *P1* and *P2* are shown in Figure 2. The wave height spectrum observed by the buoy has a single, sharp peak at 0.12 Hz, in approximate accordance with the observed wind history of the previous 12 hours. The significant wave height was 3.4 m, consistent with the higher wind speed. As mentioned above, the indicated direction of the dominant waves had been set to about 330° to be consistent with the earlier winds. Wave directions in the range 0.2–0.3 Hz were indicated by the buoy to be parallel to the wind, while higher-frequency waves were to the west. Each estimate of *P* has a single major peak near 0.12 Hz.

The bump in the wave height spectrum at 0.07–0.08 Hz is, by itself, not of major significance. However, this bump and observations that the wave directions near 70°–80° differed from the others and that the *P* plots showed local peaks near that frequency indicate the buoy to have recorded a swell moving east through the region.

The two SLAR images were processed to two-dimensional wave number spectra, Figures 3a and 4a, and directional spectra at series of frequencies, Figures 3b and 4b. The radially symmetric wave number plots distinguish separate wave

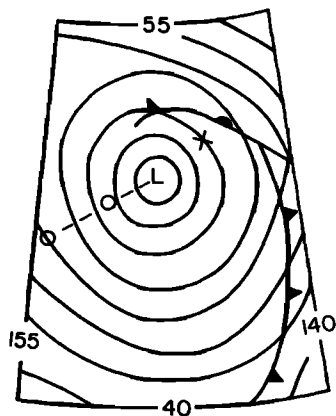


Fig. 1. Surface pressure weather chart for 1800 UT November 17, 1978, south of Alaska. The track of the storm center over the previous 12 hours and the location of the wave measurements are marked.

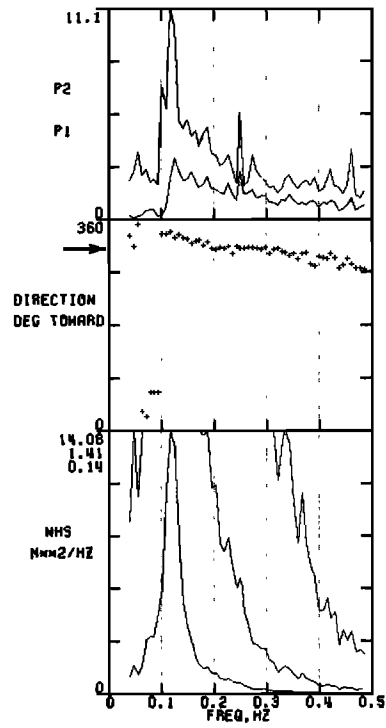


Fig. 2. Wave measurements from buoy. The wave height spectrum at three vertical scales, mean direction, and cosine directional distribution exponents *P1* (below) and *P2* (above) are shown at 1/128-Hz frequency intervals. The wind direction is shown to be toward 310°.

groups, while the directional plots reveal more readily frequencies of the maxima, mean directions and widths of the dominant peaks at each frequency, and the general background level. Similar patterns were recorded in the two cases even though the data were collected at locations 40 km apart and the aircraft headings at the two times were 99° different. The angle between the major wave propagation direction and the radar beam directions was 60°–80° in one case and 20°–40° in the other. The spectra show no trend toward lower values near the sides of the plots (azimuth directions), and no major influence of a directional transfer function is apparent. The mean directions of the wave peaks at each frequency as given by radar are close to those from the buoy; they are seen in Figure 5 to undergo similar and significant overall change with frequency. The standard deviation of the radar-buoy differences in that figure is 6° as compared with a maximum difference of the buoy values of 20°.

The two sets of *P* values in Figure 2 are not close but differ by factors greater than 2. These values, obtained from the buoy data through the assumption of a cosine power shape directional distribution, show the actual shape of the directional spectrum to be different. However, a cosine power shape for the spectrum of a wave group seems probable. Other buoy data have fit it [*Longuet-Higgins et al.*, 1963], and directional spectra from radars show approximately such a shape near the frequency of the spectrum peak. We conclude that the present buoy spectrum appears to contain one or more additional variance components which lead to a different directional shape.

One additional component might consist of reverse waves, those propagating in directions opposite to the main waves.

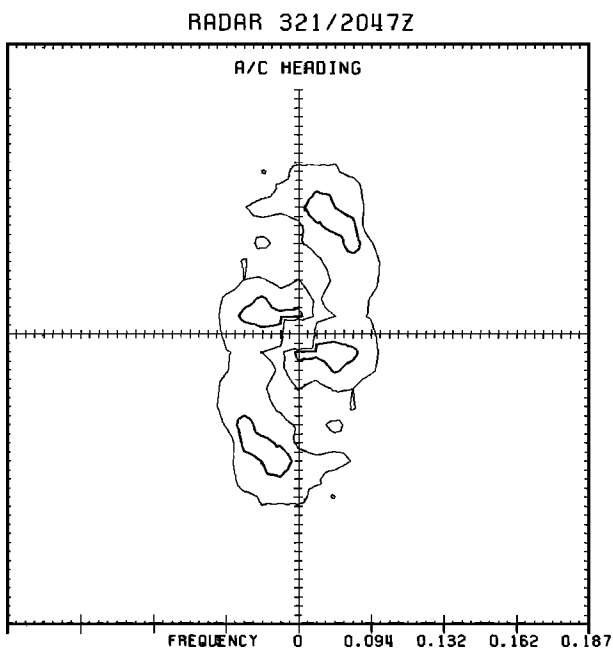


Fig. 3a. Two-dimensional wave number spectrum from airborne radar at 2047 UT. Two dots give the location of the maximum, and contours represent 50% and 25% of it. A nonlinear frequency scale corresponds to the wave numbers. Z = UT.

Indeed, Doppler radars have shown small amounts of reverse waves. *Crombie et al.* [1978] reported 1–4% of the energy of the dominant waves to be traveling in the opposite direction. The reverse waves were attributed to wave-wave interactions. These transfer wave energy to the growing low-frequency side of the spectrum peak and can produce both forward traveling and reverse waves. *Stewart and Teague* [1980] found 1% reverse wave energy which they concluded was reflected from a shore, while *Tyler et al.* [1974] recognized a 2% level of reverse waves as part of an isotropic component. However, the second component of the present buoy spectrum may not consist entirely of reverse waves. The appendix gives a method of calculating their effect on P_1 and P_2 . The calculations show that the pair of P values at 0.125 Hz in Figure 2 would represent 9% reverse waves if such were the case, a greater amount than previously detected by radar. Furthermore, the radar directional spectra of *Tyler et al.* [1974] and *McLeish et al.* [1980] show additional energy to be distributed over the entire range of directions reported, not just in reverse directions, and so could buoy spectra. It is noted that reverse waves cause a decrease in P_1 but do not change P_2 and, therefore, could be consistent with the buoy values.

Alternatively, a broad spread in direction might be approximated by an isotropic distribution, again calculated in the appendix. The level of an isotropic component in the buoy spectrum at 0.125 Hz that would give the observed behavior in P is 3% of the peak. The earlier radar measurements of 1–4% reverse wave energy are in agreement with this value, as are the background levels in a single direction of about 4% in the present radar data. Also, both the buoy and the radar spectra must contain instrument noise which need not be oriented with the waves. Other directional shapes could also cause P_1 not to be close to P_2 . However, except at the few frequencies where crossing wave trains overlap, various considerations indicate most such shapes to be improbable.

Peak width values from radar and from buoy measurements of ocean waves represent somewhat different properties of the directional distribution. A width value from radar data represents a directional peak alone, as seen through an incompletely determined transfer function. Only under the restricted conditions described above need its influence be small. In contrast, a buoy-derived width represents the cosine power shape that best fits the entire directional spectrum. The fit is influenced by all waves at the frequency, not just the dominant peak. Comparison of width values from the two instruments is therefore not straightforward.

Figure 6 presents a comparison of calculated directional

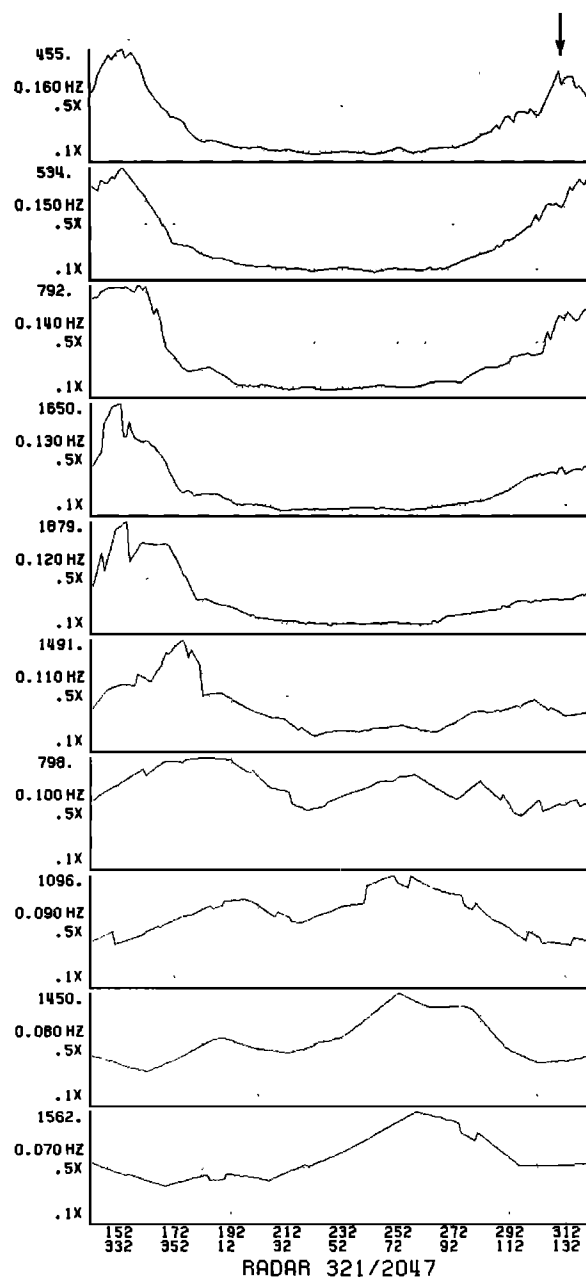


Fig. 3b. Directional spectrum from airborne radar at 2047 UT. The two direction scales along the bottom represent the two directions represented by each variance value. The radar range direction is in the center of the horizontal axis. The value of the peak in each plot is given to the upper left. Reference dotted lines show 0.1 and 0.5 times the peak value. The arrow at the top shows wind direction.

widths from the buoy at frequencies containing a single dominant wave group (as shown by radar) with measured values from the radar. Directional widths from the two radar spectra are nearly the same and do not show an influence from the different aircraft headings. Three plots of buoy-derived widths shown in Figure 6 represent different sets of estimates of P . The values in the top line were derived from P_1 and are somewhat greater than those deduced from corresponding P values by *Forristall et al.* [1978]. The second (next lower) curve, showing results derived from P_2 , represents wave peak widths if the differences between P_1 and P_2 result from reverse waves. The last buoy curve represents widths if the differences between P_1 and P_2 result from an isotropic additional component. At frequencies between 0.10 Hz and 0.12 Hz, isotropic calculations fail, and a different component, possibly reverse waves, must be present in the developing region of the spectrum.

Even the buoy widths assuming an isotropic component are an average of 25° greater than the radar values, although they had been corrected for extraneous variance in the buoy data. Compass errors in the buoy data occur when the buoy tilts on a wave and the swinging compass container jerks against its tether. These errors widen a directional peak, although inherently not as a function of frequency. The slope of the rms fit of the narrowest buoy widths versus frequency is within 15% of that from the radar and so is in accord with the predicted effect of random compass errors. This figure not only supports the accuracy of the present radar calculations but also indicates wave distributions to be narrower than previously reported buoy results [e.g., *Mitsuyasu et al.*, 1975].

The buoy data describe the dominant waves as having a peak at 0.12 Hz with a single mean direction. In contrast, directional distributions from both radar spectra show two peaks at that frequency, separated in direction by about 20° . A wave group toward 350° appears in both sets of radar distributions at the peak frequency and at a few lower frequencies. Waves toward 330° appear in both sets at and a few frequencies above the peak frequency. Because of uncertainties in the probability

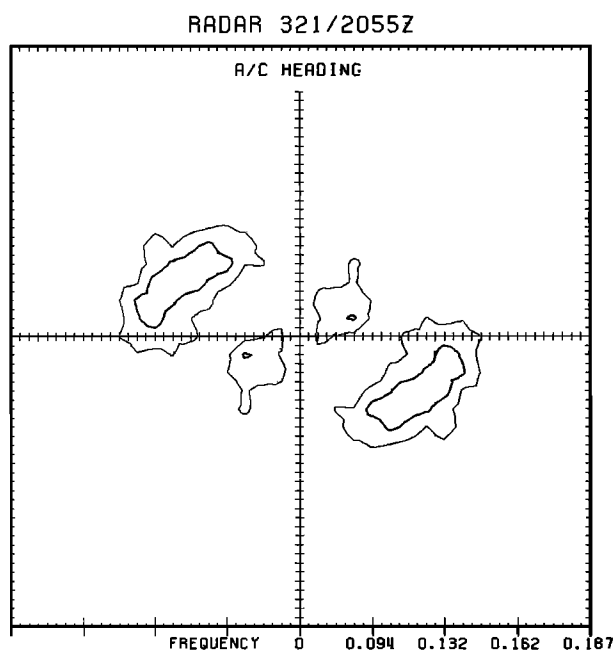


Fig. 4a. Two-dimensional wave number spectrum from airborne radar at 2055 UT.

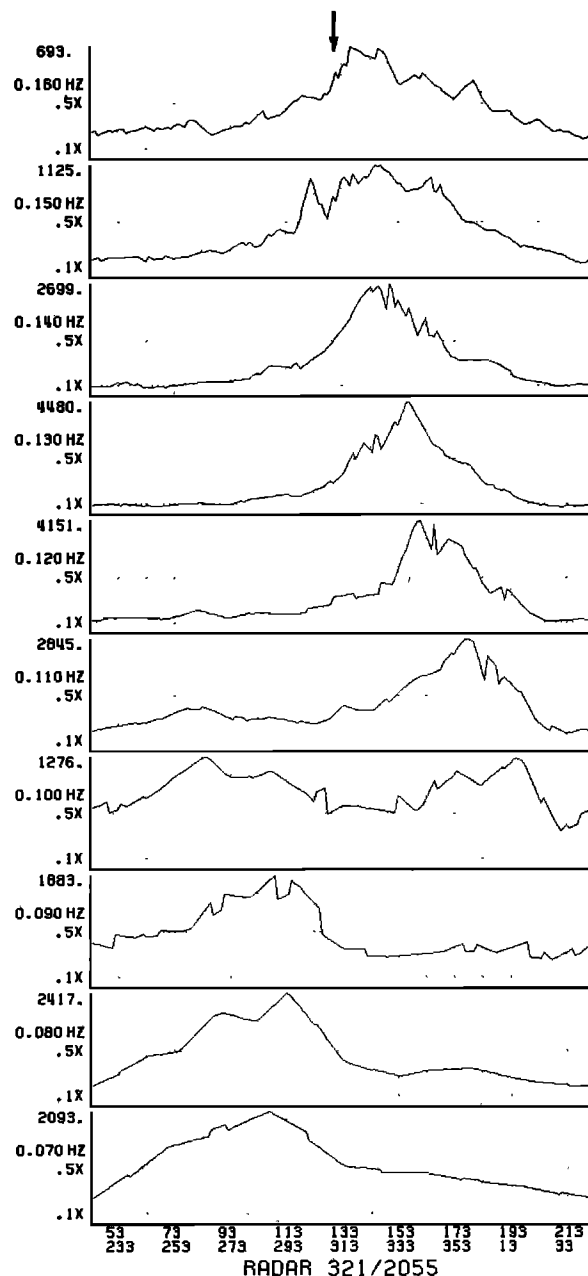


Fig. 4b. Directional spectrum from airborne radar at 2055 UT.

structure of the wave field, it is difficult to evaluate quantitatively the likelihood that the separate peaks in the radar spectra represent separate wave groups of the sea. They are, however, consistent with the time history of the local wind conditions described earlier. The existence of this double peak is supported not only by its occurrence in two separated images but also by its repetition at independent adjacent frequencies and the consistent changes between them. *Belousov et al.* [1982] reported a radar image to contain two groups of waves at overlapping frequencies in directions 37° apart. The widths of the two peaks were 35° and 40° .

As seen in Figure 5, the radar peak changed direction with frequency, and some of the variance at 0.16 Hz was nearly parallel to the wind direction (toward 310°). However, other energy toward 330° also is present at that frequency in the radar distributions.

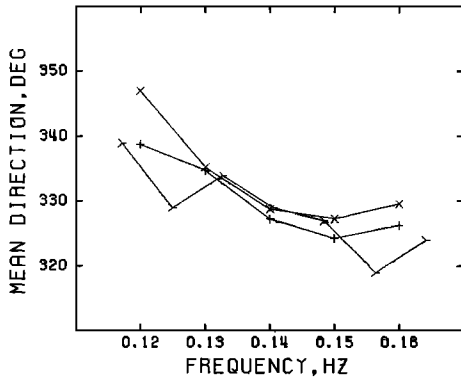


Fig. 5. Mean direction of wave peak versus frequency in storm south of Alaska. Radar measurements at 2047 UT (pluses) and at 2055 UT (crosses) are compared with buoy measurements (arrows).

The 0.07- to 0.08-Hz east-moving swell barely detectable in the buoy data constituted the dominant waves over that frequency range in the radar distributions. This energy may have come from a storm 3000 km to the west which had generated such waves 3 days earlier. Weather charts for the time period indicated that the generating area was no more than 800 km wide, so that a directional width of 15° or less would be expected, in contrast to the indicated 60°–70°. In principle, a swell can be scattered as it propagates across the ocean surface, and the directional width increased. However, *Snodgrass et al.* [1966] deduced the effect to be small, and *Munk et al.* [1963] estimated peak widths of less than 14°–37° in waves that had traveled much farther than these. It is not known whether the greater width of this peak results from some property of radar measurements of the low swell or from actual scattering of the waves in passing through the steep waves and the currents in the storm.

SATELLITE OBSERVATIONS OF WAVES FROM HURRICANE FICO

Waves generated by a hurricane offer several advantages for the study of radar patterns and of wave properties. The source

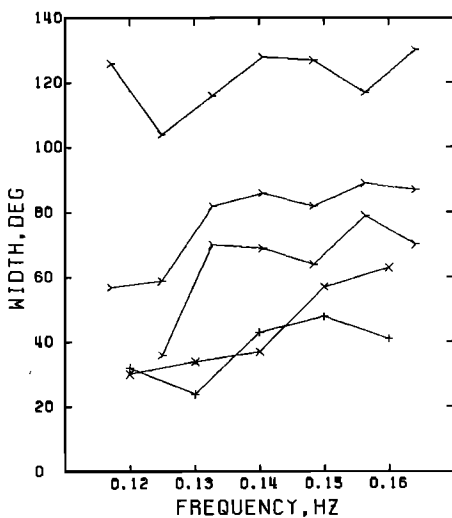


Fig. 6. Width of wave peak in storm south of Alaska versus frequency. Symbols as in Figure 5, but top buoy curve was derived from P1, next curve from P2, and third curve with equations in the appendix.

of the waves is compact and reasonably well located in time and space. The generation region is delimited by the maximum and minimum radii of wind speeds high enough for wave generation and by the rapid change of wind direction with distance around the storm. Yet the winds are sufficiently intense to generate waves, even in the short fetch, that lead to a sea or swell adequate for measurement. The hurricane may move rapidly in comparison with the scale of the storm and the wave travel time, and the strong winds follow highly curved tracks. As a result, the mean directions of the waves vary significantly across a limited portion of the ocean surface. In contrast, large-scale wind systems may generate waves that have little variation in direction over distances to be considered here. Moreover, not only were most appropriate northern hemisphere storms at incorrect distances to produce extraneous swell, but the northeast trade winds in the region were light and variable during the observation period. On the other hand, the direction of wave energy in a hurricane cannot be predicted accurately because of the rapidly changing winds and the strong wave-wave interactions occurring among the many crossing waves. Also, there are seldom many ship reports within a hurricane to aid in determining the wind distribution.

Figure 7 shows the approximate winds and significant wave heights in the vicinity of Hurricane Fico and the regions of three SAR images. When SEASAT passed at 1330 UT July 14, 1978, the eye was at 14.9°N, 121.9°W. The hurricane had been moving west at 5 m/s with a maximum sustained wind speed near 40 m/s and a radius to maximum wind estimated to be 60–70 km [Ross et al., 1983]. The speed of the hurricane motion was equal to the group velocity of waves with a frequency of 0.16 Hz. In contrast with the previous example, the bulk of the energy of the waves examined here outran the storm and was moving forward away from the generating area.

Figures 8–10 contain directional spectra in the three regions derived from averages of the two-dimensional spectra calculated at 12 subsections in each region. The spectra at different distances from the storm have significantly different characteristics. However, the high-frequency portions of the spectra in all three regions contain a narrow peak superimposed on a fairly large uniform background. Each peak is in the range direction

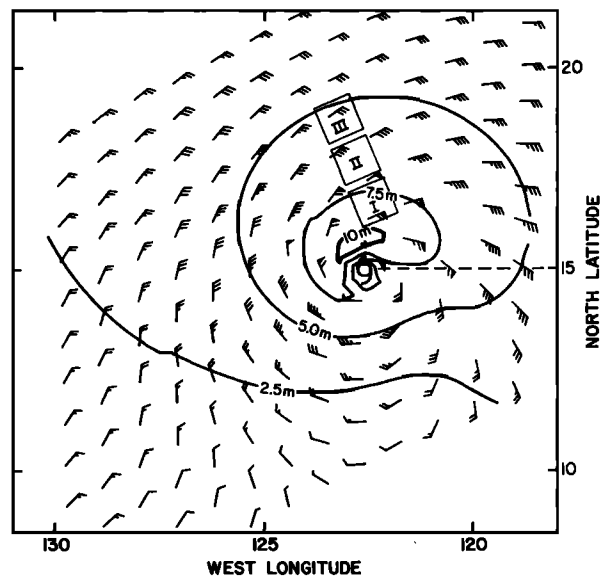


Fig. 7. Winds and waves near Hurricane Fico at 1300 UT July 14, 1978 [after Teleki et al., 1979]. The three regions of radar images and the hurricane track are marked.

of 250° and is about 20° from the wind direction given by a numerical wind model of the hurricane of Ross *et al.* [1983]. Its width is much less than previously reported for high-frequency waves beneath hurricane winds [Forristall *et al.*, 1978]. Acceleration of reflecting elements on waves moving in range causes smearing in the azimuth direction on a SAR image [Alpers *et al.*, 1981], which may lead to spectrum variance in the range direction. These inconsonant aspects of the high-frequency portions of the SAR spectra thus might represent an aspect of the system performance and not directly the waves. The total variance of the peaks in the frequency range 0.13–0.17 Hz is nearly 3 times as great in region I as in region III, a probable result of the different wind speeds.

The maximum energy in Figure 10 occurs at 0.08 Hz with a well-defined directional peak and represents a dispersed swell in the most distant area recorded. The directional peaks containing maximum energy in the areas nearer the storm in Figures 8 and 9 are less well defined. Some of the additional low-frequency variance in those figures might result from extraneous swell that was generated in distant storms. Examination of earlier weather maps and calculation of wave energy travel time indicate that various wave groups arriving from 200°–230° in the frequency range 0.06–0.09 Hz could have come from high-latitude southern hemisphere winter storms after having traveled 10–13 days [cf. Cartwright *et al.*, 1977]. Similarly, a storm near the Aleutian Islands might have generated a swell that after 7 days would arrive from 310°, the approximate direction toward which some Fico swell is seen to propagate. Ross *et al.* [1983] compared the present radar spectra with wave spectra predicted by a numerical model. The model spectra did not contain the additional swell. The contaminants were energetic enough in relation to the hurricane waves in regions I and II so that the directions and widths of the hurricane-associated peaks could not be examined in those areas. In region III, however, the sharp low-frequency peak extended well above the interference and could be measured accurately.

A mean direction was determined subjectively for each of the individual spectra in the third image at several frequencies, and the averages of 12 readings were plotted versus frequency in Figure 11. The scatter of the points from a smooth curve is much less than the overall direction change. The concave curvature in Figure 5 could not be examined at low frequencies because of apparent swell from an unrelated storm. In this figure, however, both concave and convex curvature are seen and are attributed to a single cyclone. The concave curvature over much of the frequency range can be attributed to the curving wind flow about the cyclone, but the break giving an opposite curvature at lowest frequencies is attributed to a swell emitted earlier from the moving region of high winds in the storm. The turning of the swell with frequency can be correlated with the movement of the hurricane. Figure 12 shows directional plots of the swell at the single farthest location in the third image with frequency intervals of 0.002 Hz. At this small separation, some of the variance values at adjacent frequencies are interpolated within the same sets of wave number values in the two-dimensional spectrum and are not independent. However, the consistency of shape and steadiness of changes over the series of plots indicate that even somewhat minor features of the plots may be significant. Widths are as small as 11°, and some background levels are less than 5% of the peak. The energy in the radar spectrum has a frequency bandwidth of only 0.02 Hz. Detailed analysis of these wave directions seems possible.

A simple manner of wave emission from a hurricane is assumed for evaluation of the radar observations. A wave train is 'emitted' perpendicular to a radius from the eye, with a maximum energy at a distance referred to as the 'radius of maximum

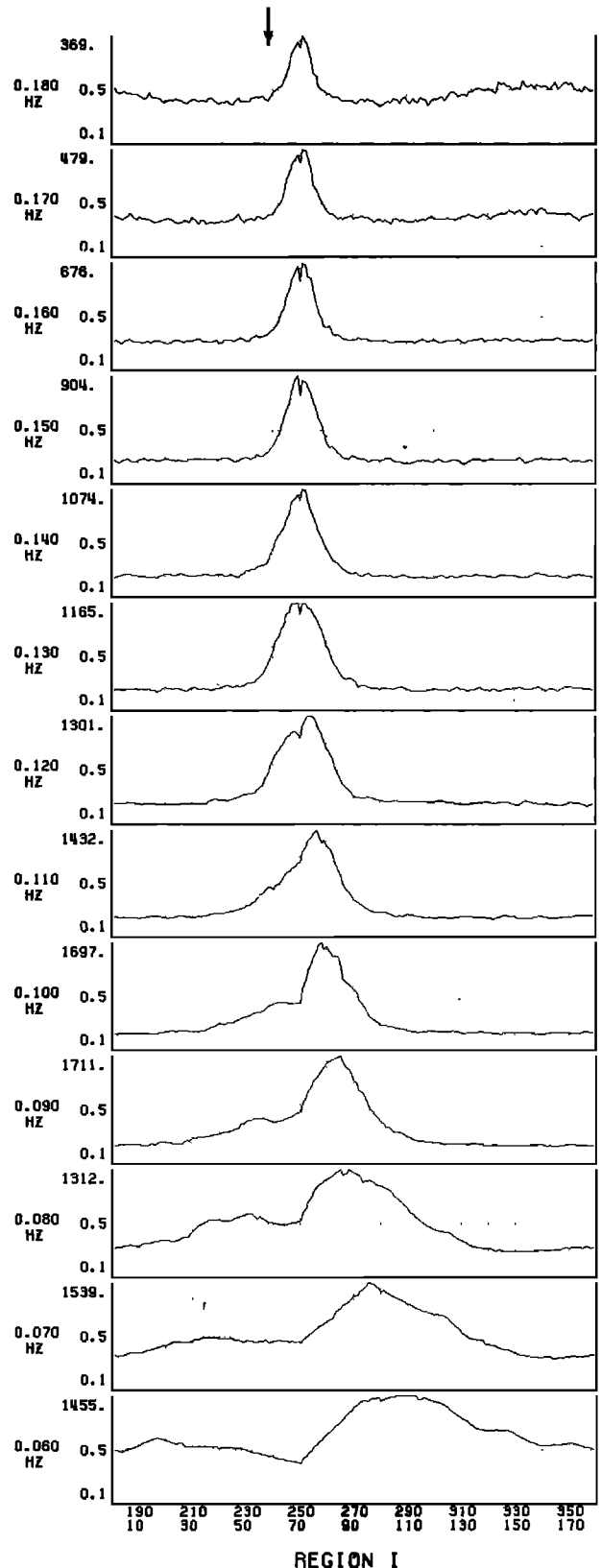


Fig. 8. Mean directional spectrum from first SEASAT radar image at location given in Figure 7. The arrow at the top shows wind direction.

waves.' The use of this approach with the present data is supported by observations of *Elachi et al.* [1977]; the dominant waves ahead of an earlier hurricane moved nearly in the storm direction, and those behind the eye often moved across the

track. But waves near the radius of maximum wind were nearly perpendicular to the radius, and those ahead and to the right of the storm were oriented in accord with this description. Furthermore, the waves are considered to travel in accord with

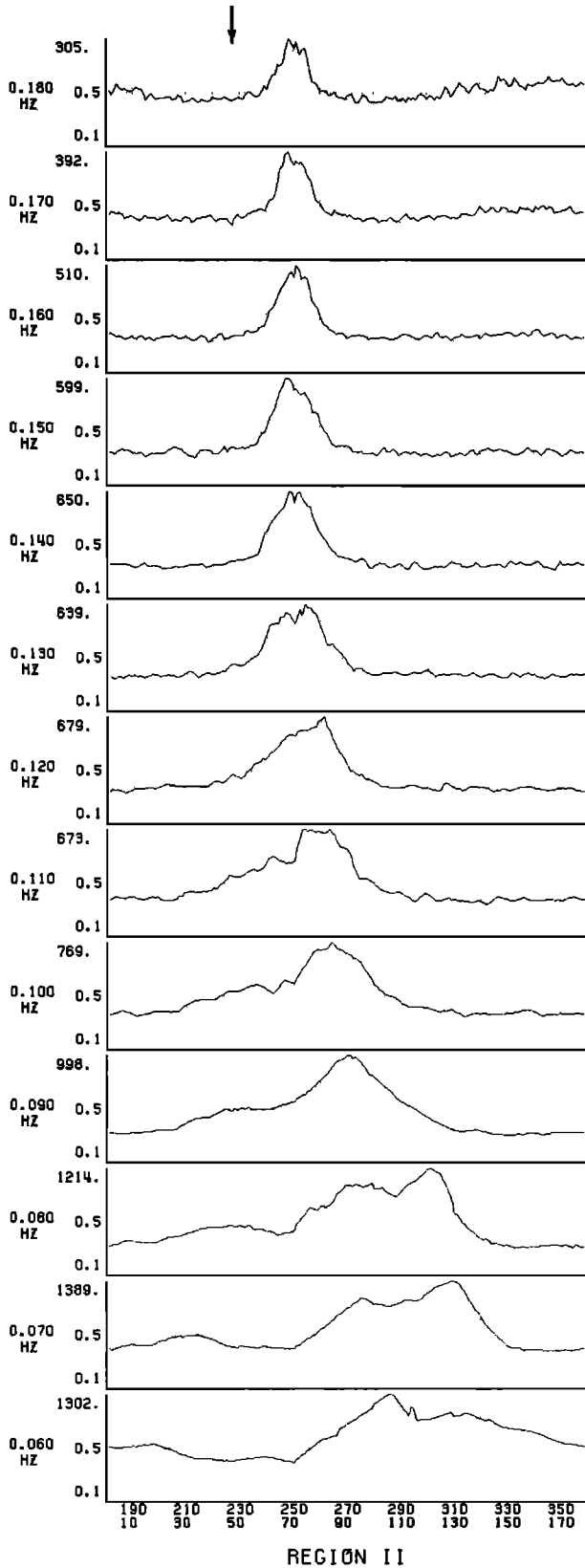


Fig. 9. Mean directional spectrum from second SEASAT radar image at location given in Figure 7.

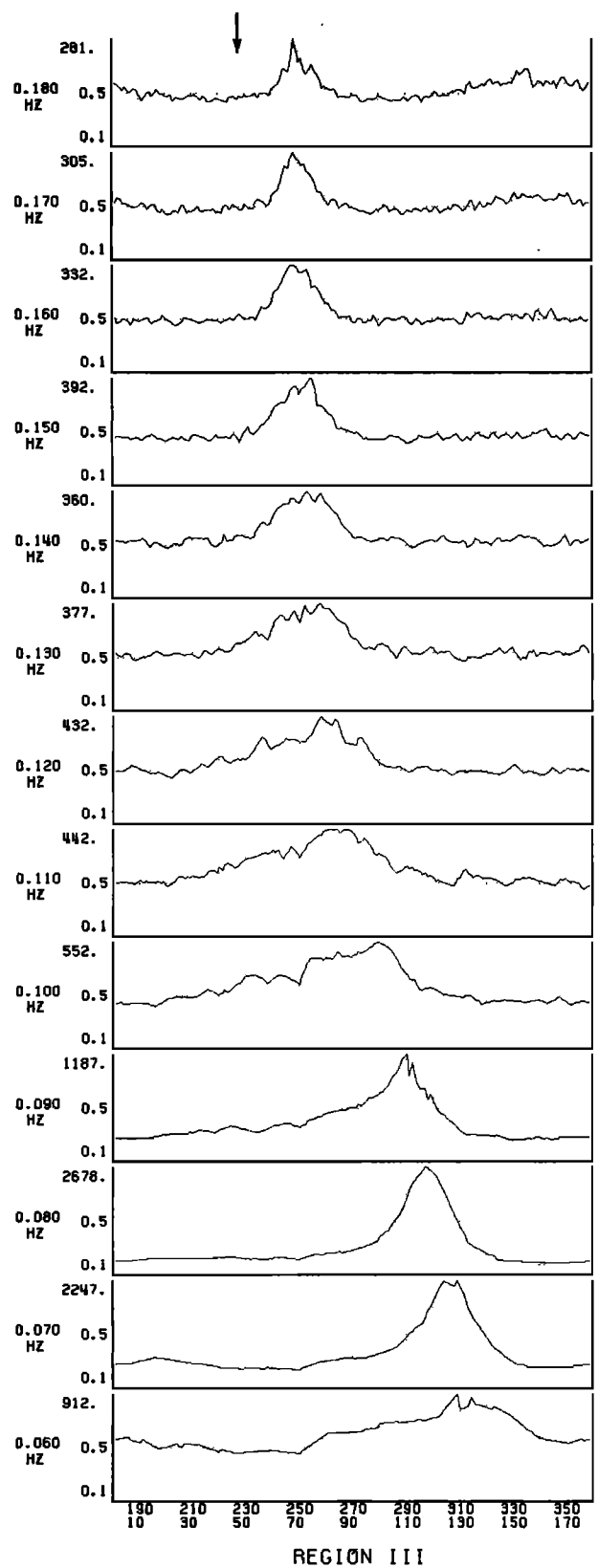


Fig. 10. Mean directional spectrum from third SEASAT radar image at location given in Figure 7.

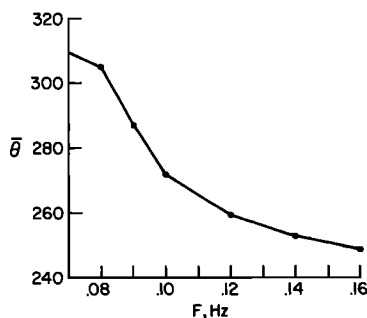


Fig. 11. Mean direction from the 12 locations in the third image versus frequency.

linear wave theory. *Snodgrass et al.* [1966] reported swells to travel great distances across the ocean in good accord with that theory and with little dissipation.

With these assumptions, the turning with frequency of the swell can be compared with the measured speed of the hurricane. Directional distributions at low frequencies from the 12 spectra from the third image were recalculated at 0.002-Hz frequency intervals, and mean wave directions were obtained. Radar geometry corrections were applied, and the 12 values at each frequency were averaged. A straight line fitted to the values at six frequencies changed direction by 4.31° between 0.070 Hz and 0.080 Hz and had an rms difference from those values of 0.16°. The trajectories of these two wave trains and the hurricane direction of motion constituted a triangle with known angles and with lengths of the sides proportional to the distances traveled. The triangle was solved numerically for relative lengths of the sides. Equating the travel times of the first wave train with the sum of that of the second wave train and that of the hurricane gave a calculated speed of the hurricane of 5.56 m/s or about 10% different from the observed value. The exact direction of hurricane advance is not critical to this calculation, nor are absolute wave directions. A difference of 10° would give a value of hurricane speed differing by ½ m/s, less than other possible errors. However, the amount of wave turning with frequency is critical. Even a 1° difference in turning leads to a hurricane speed difference of nearly 1 m/s, which could reveal a discrepancy in the data. The closeness of the calculation illustrates the high accuracy of the direction values derived from the SAR.

The average wave direction and the hurricane eye positions were combined to indicate the location of the source of the 0.078-Hz waves. These data, when considered in conjunction with the wave group velocity, indicated that the swell in the center of the northern radar image had originated at a distance of 90 km from the center of the storm and the wave energy had propagated about 550 km by observation time. These waves had traveled for 15 hours, while others in the image had traveled as much as 3 hours longer or shorter. In comparison, *Black* [1979] calculated wave origin distances of 100–250 km from the center of a major hurricane. The distance to maximum waves can hardly be less than the radius to maximum winds or so great that the wind speeds are too low to generate such waves. Thus, the present calculation implies some degree of accuracy of mean wave direction measurements. An error of ± 5° in the present values leads to distances of 40 and 145 km, and the direction error must be less.

The mean direction of 0.078-Hz waves at each of the 12 locations on the third radar image is marked at the corresponding point in Figure 13. The resulting thematic map represents

the spreading over the ocean surface of the directions of waves from a small moving storm. Gently curving contour lines show the overall change in direction to be much larger than the random scatter of the values. The assumption of a small unchanging generation region moving steadily with the storm, combined with the position of the wave source derived from the radar data, requires that the contour lines be a fan-shaped array radiating from the position of the source at observation time, as shown in the figure. The rms difference between the direction values and those from the fan array is only 2.6°. Although the observed directions fit reasonably well, significant departures of the curved contours show that hurricane wave emission is not fully as assumed. Fluctuations in the wind field around the storm and in the hurricane movement may have caused some of the differences.

Measurements of the horizontal patterns of wave directions now becoming available can be highly valuable in showing how waves vary with distance. *Shuchman and Kasischke* [1981] plotted wave orthogonals from radar over an area and compared them with those from refraction theory. *Beal* [1981] showed that wave directions along a line were consistent with a presumed source 500 km away. In the present study, the source is relatively small and moving with a component transverse to the wave direction, and further details of the wave pattern may be deduced from the radar measurements.

The thematic map in Figure 14 shows the widths of the directional peak of 0.078-Hz waves at 11 locations in area III. Comparison of the values with the smoothly curved contours indicates the random variability to be small in comparison with the overall change in width. Also, the overall change is comparable with what may be predicted. The travel times of 12 and 18 hours to the nearest and farthest locations should lead to a ratio of widths of the order of 1.5. The observed ratio is 1.8, or only 20% different. Predicted contours curve slightly in the

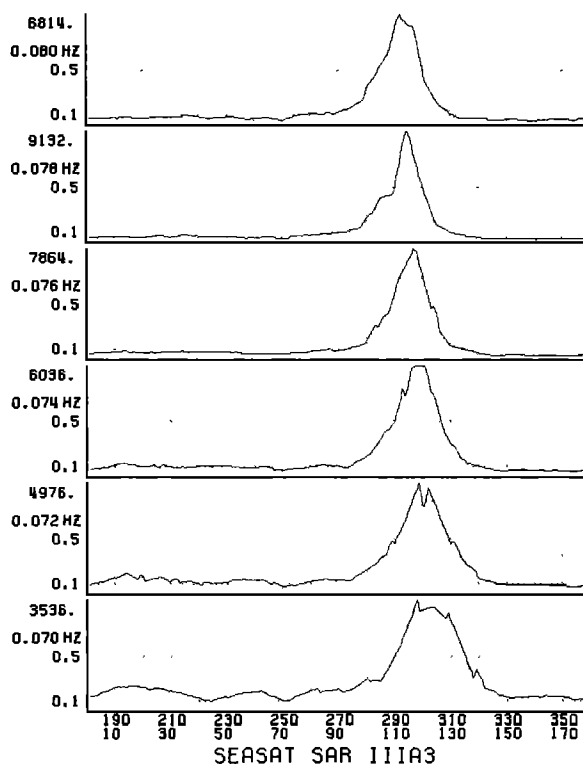


Fig. 12. Directional spectrum from satellite radar at close frequency intervals. The location is shown in Figure 14.

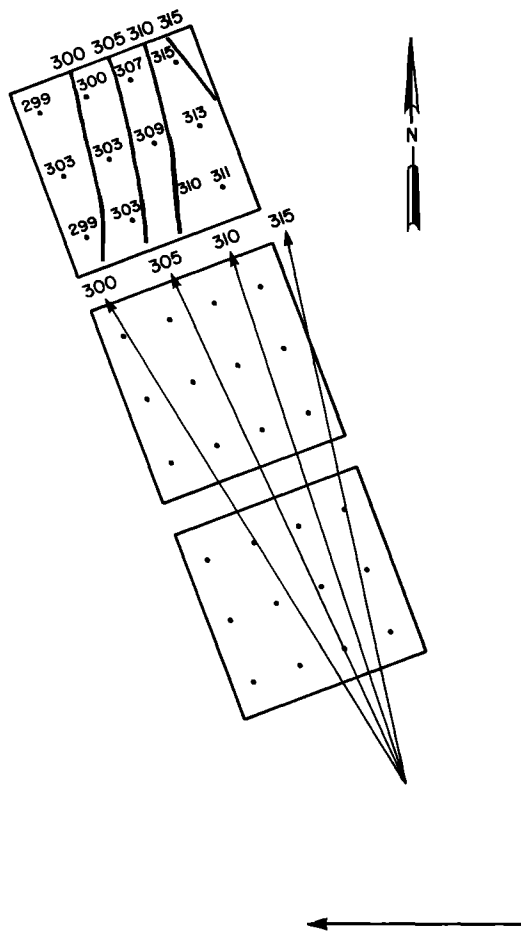


Fig. 13. Distribution over the area in the third image of the mean directions of 0.078-Hz waves. The hurricane track follows the arrow along the bottom. The curved lines in the third image represent an approximate contouring of the directions, and the fan-shaped array of straight lines represents predicted directions.

opposite direction, and the different observed patterns of the contours must result from properties of the wave emission from a hurricane not recognized at present.

The observed widths of the directional properties of the spectra can also yield information on the characteristics of the generation region of the storm. The average of the 11 radar-derived directional widths from the northernmost region (III of Figure 14) at 0.078 Hz is 17.2°. For a travel distance of 550 km, an angular spread of 17.2° implies a generation region for these waves 165 km wide. The narrowest spread in region III was 11° and represents a generation region of 125 km in width. Since the directional properties were observed to be symmetric, twice the 90-km distance from the eye to the peak generation arrived at previously would represent an independent estimate of the maximum width of the region. Thus, the directional widths observed in the spectra are consistent with an otherwise inferred width of the generation region.

Figure 15 shows the manner in which waves changed with distance from a hurricane. Low-frequency 0.078-Hz waves were examined, since dispersal is more rapid and development of new waves is slower than at higher frequencies. Directional distributions at each spectrum location along the west side of the area extending north from the storm are combined in the single figure. As the plots in Figure 12 show, a well-dispersed swell gives a single, clear-cut peak which, in the present obser-

uations, is nearly triangular. The simple description of hurricane wave emission mentioned above would require the width of a peak to increase steadily and possibly change direction as the storm was approached, but otherwise it would maintain its original shape. The calculations of fetch width from Figure 14 were based on that concept. However, the observations of the transition between swell and sea waves show a somewhat different development.

The directional plots in Figure 15 represent waves along a row of locations. The swell in the northernmost plot at IIIA3 had a narrow peak toward 295°, but the waves in the southernmost plot at IA1 showed a broad spread between 220°–240° and 300°. The plots between them illustrate the manner in which the change occurred. At locations near IIIA3, the 295° waves varied irregularly in direction by about 5° and turned to about 305° by IIA1. Here another wave train, toward 270°–280°, became dominant. Indications of this second wave train are visible in the two plots above this one. Farther south, the 305° waves became weaker, and other wave trains showed varying amplitudes until at location IA1 there was a single irregular peak with a width of 60°–80°. Thus, with both swell and sea waves present, the changes in wave directions with distance from the storm consisted more of a changing of the amplitudes of different wave trains than of the turning or broadening of a single wave train.

A similar overlapping of sea and swell at individual frequencies appears from the averaged Fico spectra. Combining the 0.07-Hz and 0.08-Hz results gives a locally generated sea

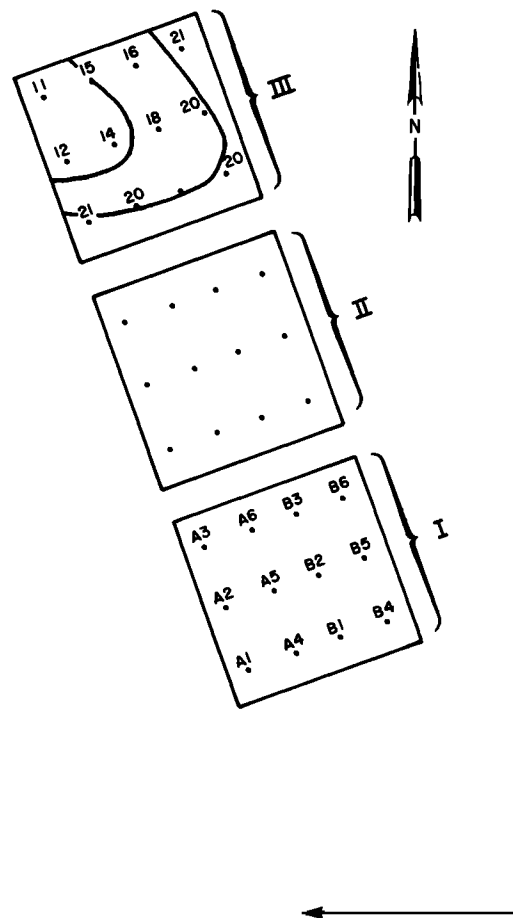


Fig. 14. Distribution over the area in the third image of the widths of the peak of 0.078-Hz waves. Locations of spectra are identified as shown along the right and within the area of the bottom image.

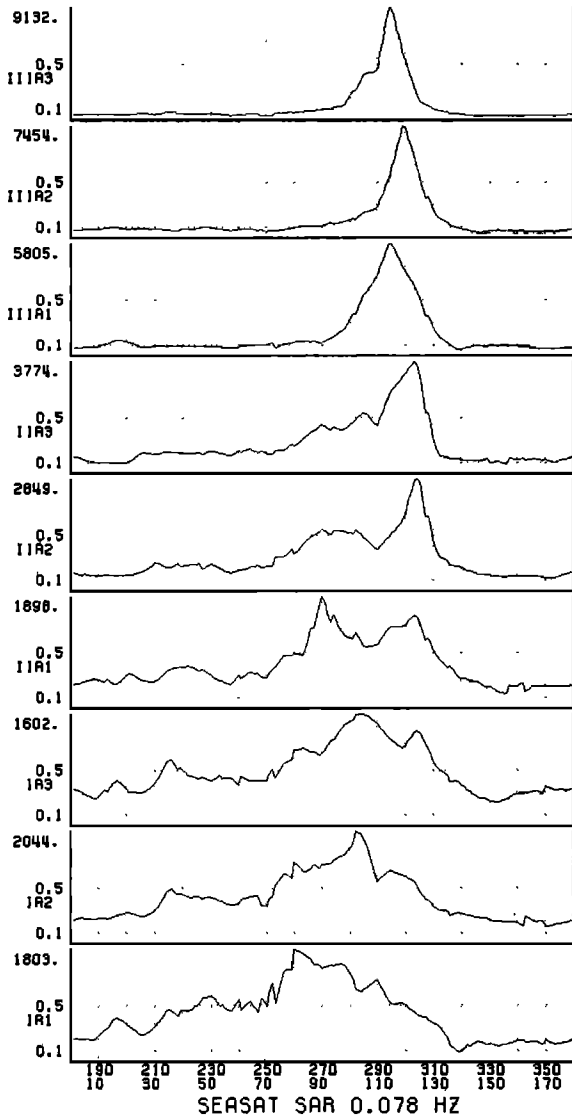


Fig. 15. Directional spectra from satellite radar at 0.078 Hz at locations in a line along the left edge of the observation area.

direction of 272° near the storm (Figure 8) and a swell direction of 302° in the farthest area (Figure 10). The intermediate distance spectrum (Figure 9) shows two peaks: sea waves toward 275° and swell waves in the direction 305°. Overlapping is also indicated by the plots at successive frequencies in Figure 9. In this example, radar observations distinguished wave groups at a single frequency which were only 30° different in direction.

Forristall *et al.* [1981] found swell from a hurricane to be separated in direction and frequency from the locally generated sea waves. The peak width of the swell may be calculated from the wave gauge and current meter data to be 35°. At intermediate frequencies, however, the *P*₁ values from such data were low, and only a broad spread, not a double peak, could be indicated.

The manner of change of directional distributions with distance as well as the shapes of the contour lines in the maps of mean wave direction and directional width is not in full accord with the present understanding of wave generation and is expected to require a more detailed examination of the winds within a hurricane and the interactions among the waves there.

Optical correlations of SAR data may show different qualities of ocean wave patterns at different ranges. In fact, *Gon-*

zalez et al. [1982] could not recognize any waves in the first quarter swath of images near Hurricane Ivy. In contrast, the present digitally correlated data gave spectra of uniform high quality across the entire set of ranges, and Figure 15 was derived entirely from the first quarter of the swath.

SUMMARY

We have examined real and synthetic aperture radar images of ocean waves with significantly different geometries and found several properties of the waves to be measured by the radars.

1. A limited range of aspects of the radar spectra was defined within which radar spectrum properties represent corresponding properties of the waves. Mean directions and widths of groups of dominant waves were derived at individual frequencies.

2. Accuracies of radar direction and width values were evaluated by comparison with in situ measurements and straightforward concepts of wave propagation. Directions of swell from a hurricane were accurate to within about 5°. Directional width values were less than those from buoy measurements but probably greater than the actual widths.

3. More detailed analysis of the radar data allowed further deductions concerning the hurricane waves to be made. (1) With the hurricane known to be moving west, its speed was calculated from the wave directions at different frequencies. (2) With the hurricane position known with other observations from the satellite, wave travel distance, travel time, and difference in travel time across a radar image were calculated. (3) Distance from the center of the storm to the generation area of maximum waves was calculated to be 90 km, in accord with an estimated radius of maximum winds of 60–70 km. (4) Both mean wave direction and directional width at a frequency varied over a 100 km square area in general accord with predictions from the hurricane. However, both showed definite departures that are attributed to variations in the hurricane winds or in the wave generation process. (5) Locally generated wind waves were distinguished from a swell through changes with distance and frequency.

APPENDIX

Directional properties of a measured wave spectrum at a frequency may be examined through its partial Fourier transform. With a coordinate system aligned with the mean direction of the dominant waves, the Fourier coefficients are

$$A_{nx} = \int_0^{2\pi} E_x(\theta) \cos(n\theta) d\theta \quad (1)$$

where *n* is the harmonic number, *n* = 0, 1, 2 here, and *X* represents the particular spectrum or component. In the present analysis, *X* may designate the dominant wave group *F* with a spectrum directional shape $E_F(\theta) = [\cos^{2P}(\theta/2)]$; reverse waves *R* with $E_R(\theta) = E_F(\theta + \pi)$ so that the spreading exponent $P_R = P_F$; an isotropic background *B* so that $A_{1B} = A_{2B} = 0$; or the sum of the components, *S*. The amounts of the lesser components may be expressed by

$$M_R = A_{0R}/A_{0F} = -A_{1R}/A_{1F} = A_{2R}/A_{2F}$$

$$M_B = A_{0B}/A_{0F}$$

so that the Fourier coefficients of the total spectrum are

$$A_{0S} = A_{0F} + A_{0R} + A_{0B} = A_{0F}(1 + M_R + M_B) \quad (2)$$

$$A_{1S} = A_{1F} + A_{1R} = A_{1F}(1 - M_R) \quad (3)$$

$$A_{2S} = A_{2F} + A_{2R} = A_{2F}(1 + M_R) \quad (4)$$

and so

$$\frac{A_{1S}}{A_{0S}} = \frac{A_{1F}}{A_{0F}} \frac{1 - M_R}{1 + M_R + M_B} \quad (5)$$

$$\frac{A_{2S}}{A_{0S}} = \frac{A_{2F}}{A_{0F}} \frac{1 + M_R}{1 + M_R + M_B} \quad (6)$$

The quantities on the left are derived from buoy measurements through LCS [Longuet-Higgins *et al.*, 1963] calculations. The cosine exponent P is related to the Fourier ratios by Cartwright [1963, Equation 17]:

$$\frac{A_{1F}}{A_{0F}} = \frac{P}{P + 1} \quad (7)$$

$$\frac{A_{2F}}{A_{0F}} = \frac{P}{P + 1} \frac{P - 1}{P + 2} \quad (8)$$

Thus

$$\frac{P}{P + 1} = \frac{A_{1S}}{A_{0S}} \frac{1 + M_R + M_B}{1 - M_R} \quad (9)$$

$$\frac{P}{P + 1} \frac{P - 1}{P + 2} = \frac{A_{2S}}{A_{0S}} \frac{1 + M_R + M_B}{1 + M_R} \quad (10)$$

These equations allow P to be determined if M_R or M_B is known.

If $M_B = 0$, P may be calculated with (10), and then M_R with (9).

If instead $M_R = 0$, (7) and (8) lead to

$$P = \left(1 + \frac{2A_{2S}/A_{0S}}{A_{1S}/A_{0S}} \right) \left(1 - \frac{A_{2S}/A_{0S}}{A_{1S}/A_{0S}} \right)^{-1} \quad (11)$$

Next, M_B is evaluated with (9):

$$M_B = \frac{P}{(P + 1)A_{1S}/A_{0S}} - 1 \quad (12)$$

Calculation of the height of the background relative to that of the dominant wave peak uses [Cartwright, 1963, Equations 14 and 15]

$$H_B = \frac{M_B}{2\pi} \frac{\pi\Gamma(2P + 1)}{2^{2P-1}\Gamma^2(P + 1)} \quad (13)$$

Equations (11) to (13) provided the buoy values in the discussion above. This approach is somewhat more general than the LCS method in that it can give correct values of P with an isotropic background, although any discrepancies will not be apparent in the results. These equations emphasize the importance of knowledge of the different components in a spectrum.

Acknowledgments. Financial support was provided by the SEASAT project office of NESS. The SEASAT radar measurements near Hurricane Fico were calculated through a digital correlation by C. Wu of the Jet Propulsion Laboratory. The airborne radar was operated by J. Tomchay and R. Berles, and the buoy measurements were obtained by B. Gritton. Opportunity to make buoy measurements from the ship was provided by the Canadian Coast Guard. R. B. Long provided valuable comments on the manuscript, and J. Ewing showed limitations to the analysis in the appendix.

REFERENCES

Alpers, W. R., D. B. Ross, and C. L. Rufenach, On the detectability of ocean surface waves by real and synthetic aperture radar, *J. Geophys. Res.*, **86**, 6481–6498, 1981.

- Beal, R. C., Spatial evolution of ocean wave spectra, in *Spaceborne Synthetic Aperture Radar for Oceanography*, edited by R. C. Beal, P. S. DeLeonibus, and I. Katz, pp. 110–127, Johns Hopkins, Baltimore, Md., 1981.
- Belousov, P. S., E. O. Zhilko, A. A. Zagorodnikov, V. I. Kornienko, V. S. Loshchilov, and K. B. Chelyshev, Study of wind-driven sea parameters using side-looking airborne radar, in *USSR/USA Bering Sea Experiment*, edited by K. Ya. Kondrat'ev, pp. 61–72, Amerind Publishing, New Delhi, 1982.
- Black, J. L., Hurricane Eloise directional wave spectra, paper presented at Eleventh Annual Offshore Technology Conference, Dallas, 1979.
- Born, G. H., J. A. Dunne, and D. B. Lame, SEASAT mission overview, *Science*, **204**, 1405–1406, 1979.
- Cartwright, D. E., The use of directional spectra in studying the output of a wave recorder on a moving ship, in *Ocean Wave Spectra*, pp. 203–218, Prentice-Hall, Englewood Cliffs, N. J., 1963.
- Cartwright, D. E., J. S. Driver, and J. E. Tranter, Swell waves at Saint Helena related to distant storms, *Q. J. R. Meteorol. Soc.*, **103**, 655–683, 1977.
- Crombie, D. D., K. Hasselmann, and W. Sell, High-frequency radar observations of sea waves travelling in opposition to the wind, *Boundary Layer Meteorol.*, **13**, 45–54, 1978.
- Elachi, C., Radar imaging of the ocean surface, *Boundary Layer Meteorol.*, **13**, 165–179, 1978.
- Elachi, C., T. W. Thompson, and D. King, Ocean wave patterns under Hurricane Gloria: Observation with airborne synthetic-aperture radar, *Science*, **198**, 609–610, 1977.
- Forristall, G. Z., E. G. Ward, V. J. Cardone, and L. E. Borgmann, The directional spectra and kinematics of surface gravity waves in Tropical Storm Delia, *J. Phys. Oceanogr.*, **8**, 888–909, 1978.
- Forristall, G. Z., E. G. Ward, and V. J. Cardone, Directional wave spectra and wave kinematics in hurricanes Carmen and Eloise, in *Proceedings of the Seventeenth Coastal Engineering Conference*, pp. 567–586, American Society of Civil Engineers, New York, 1981.
- Gonzalez, F. I., R. C. Beal, W. E. Brown, P. S. DeLeonibus, J. W. Sherman III, J. F. R. Gower, D. Lichy, D. B. Ross, C. L. Rufenach, and R. A. Shuchman, SEASAT synthetic aperture radar: Ocean wave detection capabilities, *Science*, **204**, 1418–1421, 1979.
- Gonzalez, F. I., T. W. Thompson, W. E. Brown, Jr., and D. E. Weissman, SEASAT wind and wave observations of northeast Pacific Hurricane Iva, August 13, 1978, *J. Geophys. Res.*, **87**, 3431–3438, 1982.
- Jordan, R. L., The SEASAT-A synthetic aperture radar system, *IEEE J. Oceanic Eng.*, **OE-5**, 154–164, 1980.
- Longuet-Higgins, M. S., D. E. Cartwright, and N. D. Smith, Observations of the directional spectrum of sea waves using the motions of a floating buoy, in *Ocean Wave Spectra*, pp. 111–132, Prentice-Hall, Englewood Cliffs, N. J., 1963.
- McLeish, W., D. Ross, R. A. Shuchman, P. G. Teleki, S. V. Hsiao, O. H. Shemdin, and W. E. Brown, Jr., Synthetic aperture radar imaging of ocean waves: Comparison with wave measurements, *J. Geophys. Res.*, **85**, 5003–5011, 1980.
- Meadows, G. A., R. A. Shuchman, Y. C. Tseng, and E. S. Kasischke, SEASAT synthetic aperture radar observations of wave-current and wave-topographic interactions, *J. Geophys. Res.*, this issue, 1983.
- Mitsuyasu, H., F. Tasai, T. Suhara, S. Mizuno, M. Ohkusu, T. Honda, and K. Rikiishi, Observations of the directional spectrum of ocean waves using a cloverleaf buoy, *J. Phys. Oceanogr.*, **5**, 750–760, 1975.
- Munk, W. H., G. R. Miller, F. E. Snodgrass, and N. F. Barber, Directional recording of swell from distant storms, *Philos. Trans. R. Soc. London, Ser. A*, **255**, 505–584, 1963.
- Pawka, S. S., S. V. Hsiao, O. H. Shemdin, and D. L. Inman, Comparisons between wave directional spectra from SAR and pressure sensor arrays, *J. Geophys. Res.*, **85**, 4987–4995, 1980.
- Rosenthal, W., R. A. Shuchman, and J. D. Lyden, SAR derived wave spectra from MARSEN, (abstract), *Eos Trans. AGU*, **62**, 931, 1981.
- Ross, D., L. M. Lawson, and W. McLeish, Comparison of Hurricane Fico winds and waves from numerical models with observations from SEASAT-A, in *Wave Dynamics and Radio Probing of the Ocean Surface*, edited by O. M. Phillips and K. Hasselmann, Plenum, New York, in press, 1983.
- Schwab, D. J., R. A. Shuchman, and P. C. Liu, Wind wave directions determined from synthetic aperture radar imagery and from a tower in Lake Michigan, *J. Geophys. Res.*, **86**, 2059–2064, 1981.
- Shuchman, R. A., and E. S. Kasischke, Refraction of coastal ocean waves, in *Spaceborne Synthetic Aperture Radar for Oceanography*, edited by R. C. Beal, P. S. DeLeonibus, and I. Katz, pp. 128–135, Johns Hopkins, Baltimore, Md., 1981.

- Shuchman, R. A., and J. S. Zelenka, Processing of ocean wave data from a synthetic aperture radar, *Boundary Layer Meteorol.*, 13, 181-191, 1978.
- Snodgrass, F. E., G. W. Groves, K. F. Hasselmann, G. R. Miller, W. H. Munk, and W. H. Powers, Propagation of ocean swell across the Pacific, *Philos. Trans. R. Soc. London, Ser. A*, 259, 431-497, 1966.
- Stewart, R. H., and C. Teague, Dekameter radar observations of ocean wave growth and decay, *J. Phys. Oceanogr.*, 10, 128-143, 1980.
- Teleki, P. G., W. J. Campbell, R. O. Ramseier, and D. Ross, The offshore environment: A perspective from SEASAT-1 SAR data, paper presented at Eleventh Annual Offshore Technology Conference, Dallas, 1979.
- Tyler, G. L., C. C. Teague, R. H. Stewart, A. M. Peterson, W. H. Munk, and J. W. Joy, Wave directional spectra from synthetic aperture observations of radio scatter, *Deep Sea Res.*, 21, 989-1016, 1974.
- Vesecky, J. F., and R. H. Stewart, The observation of ocean surface phenomena using imagery from the SEASAT synthetic aperture radar: An assessment, *J. Geophys. Res.*, 87, 3397-3430, 1982.
- Wright, J. W., W. J. Plant, W. C. Keller, and W. L. Jones, Ocean wave-radar modulation transfer functions from the West Coast Experiment, *J. Geophys. Res.*, 85, 4957-4966, 1980.
- Wu, C., B. Barkan, B. Huneycutt, C. Leang, and S. Pang, An introduction to the interim digital SAR processor and the characteristics of the associated SEASAT SAR imagery, *Publ. 81-26*, Jet. Propul. Lab., Calif. Inst. of Technol., Pasadena, 1981.

(Received February 2, 1982;
revised January 24, 1983;
accepted January 25, 1983.)